Fabrication and Characterization of High Kinetic Inductance Superconducting Resonators via Atomic Layer Etching

Yueheng Shi & Kaushal Shyamsundar
Mentors: Lavendra Mandyam, Michelle Rincon, Ke Huang

June 2, 2025

Abstract

High-kinetic-inductance superconducting resonators underpin many emerging quantum technologies, yet their performance is often limited by fabrication-induced surface damage and film roughness. We report a fully integrated workflow to pattern 20 nm niobium-nitride (NbN) films on silicon with angstrom-level precision using a cyclic SF/O atomic-layer-etch (ALE) process. Systematic metrology shows an NbN etch rate of 0.28–0.33 nm per cycle while the underlying Si etches 2 nm cycle^{1}, enabling controlled over-etch and clean sidewalls. Atomic-force-microscopy confirms sub-nanometre roughness after a post-etch oxidation/BOE clean. Quarter-wave coplanar-waveguide resonators fabricated with this process reach internal quality factors up to 1 million, demonstrating that the low-loss potential of ultrathin NbN can be retained. Our methodology—combining ALE, analytical/EM design tools, and cryogenic measurements—provides a scalable route to high-impedance resonators for next-generation qubits, microwave kinetic-inductance detectors, and hybrid quantum systems.

1 Introduction

High kinetic inductance resonators are a cornerstone technology for advancing scalable quantum circuits. Their high impedance facilitates strong coupling to qubits, enabling fast, high-fidelity quantum gates [8]. They are also of interest in condensed matter physics, because they are at the edge of the Superconductor-to-Insulator Transition [4]. Additionally, they allow for stronger coupling to electric dipoles making them ideal for coupling to quantum systems like spin qubits, and 2D materials[3].

Materials such as niobium nitride (NbN) are ideal for these applications due to their high kinetic inductance, relatively high critical temperature ($T_c \approx 12K$), and resilience in magnetic fields[9]. However, the performance of these devices, particularly their quality factor (Q), is highly sensitive to material properties and surface quality. Surface roughness, contaminants, and fabrication-induced defects can introduce significant microwave loss, thereby reducing qubit coherence times. Specifically, for applications where high kinetic inductance is required it is paramount to start with extremely thin films, since kinetic inductance scales inversely with the thickness of the superconducting material. As such, the surface roughness is doubly important when working with kinetic inductance materials. Therefore, in order to create devices from these materials one, first needs to find a way to reliably pattern them in a way that minimizes surface roughness.

Atomic Layer Etching (ALE) is an advanced fabrication technique that offers Angstrom-level control by using self-limiting chemical reactions. This project aimed to leverage ALE to pattern

NbN films with minimal surface damage, thereby preserving the intrinsic low-loss properties of the material. The goal of this project is to develop a technique to pattern high quality factor resonators on NbN thin films, approximately 20 nm thick via atomic layer etching to create high coherence resonators. The Atomic Layer etching will hopefully allow for a smoother surface after the patterning step, but will also allow for global control of the thickness of the film enabling the kinetic inductance of a sample to be tuned after growth.

2 Materials and Methods

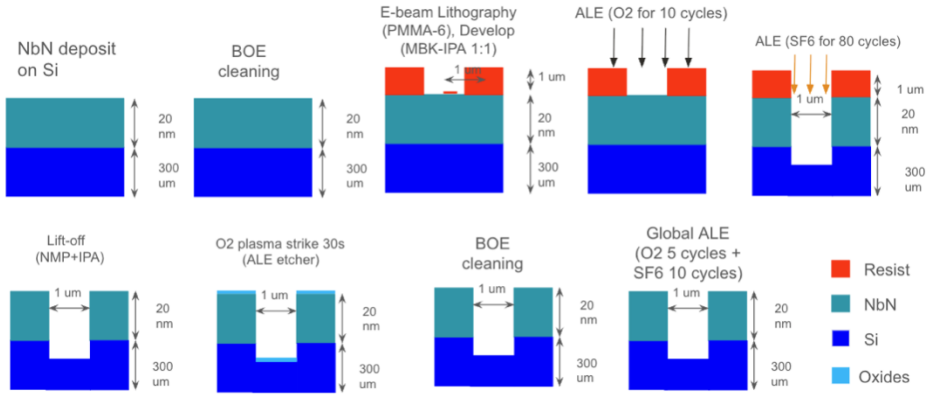

Figure 1: A schematic overview of the device fabrication workflow, illustrating the key steps from the initial deposition of Niobium Nitride (NbN) on a Silicon (Si) substrate to the final device structure after multiple lithography, etching, and cleaning processes.

2.1 Device Fabrication

A detailed, multi-step fabrication process was developed, beginning with NbN thin films on silicon wafers as shown in Fig. 1

2.1.1 Atomic Layer Deposition of NbN on Si

This step is done in the Atomic Layer Depostion (ALD) equipment by our collaborator at Yale University. ALD is deployed to ensure the surface smoothness. The recipe is not disclosed here for protecting IP but here's an example recipe of growing NbN on Si using ALD [10] [9].

2.1.2 Electron-Beam Lithography

Device patterns were defined using a standard e-beam lithography process.

- **Resist Coating:** A polymethyl methacrylate (PMMA) A6 resist was spin-coated onto the substrate at 4000 RPM and subsequently baked at 180°C for 5 minutes.
- **Pattern Exposure:** A dose of 400 $\mu C/cm^2$ at a beam current of 50 nA was used for pattern exposure. Proximity Effect Correction (PEC) was performed using the standard Beamer software procedure.

- **Development:** The exposed resist was developed in a MIBK:IPA (1:1) solution for 2.5 minutes, followed by a 1 minute 45 second dunk in pure IPA and blow dry afterwards.

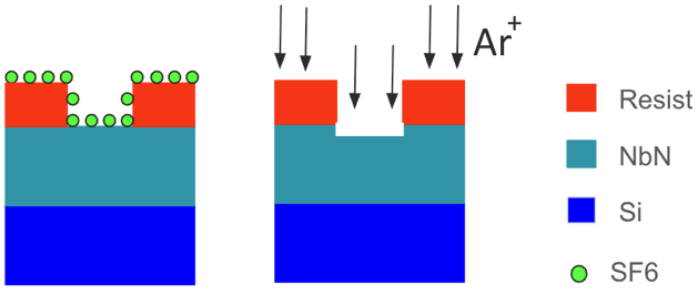

Figure 2: An illustration of the Atomic Layer Etching (ALE) mechanism for Niobium Nitride (NbN). The process involves the introduction of SF6 gas to the NbN surface, followed by an Argon (Ar+) plasma to remove the reacted material.

2.1.3 Atomic Layer Etching (ALE)

The core technological development of this project was a cyclical ALE process designed for NbN etching. Fig. 2 illustrates the ALE process of SF6 ethcing NbN: the NbN surface is covered with a monolayer of SF6. The SF6 reacts with NbN and a weak Argonne plasma is striked to blow away the reacted Si and Flourine compounds. Below are the detailed steps for the whole ALE process.

- **Chamber cleaning:** O_2 plasma cleaning at 5W for 5-10mins with a dummy wafer(depending on previous recipes run in the chamber)
- **Chamber seasoning:** Running SF_6 etching for 20 cycles with a dummy wafer
- **O_2 Resist Removal:** 10 cycles of O2 plasma celeaning at 5W to strip the residual resist on the film (See Fig. 3 c for detailed parameters)
- **SF_6 NbN etching**: 80 cycles of SF6 plasma celeaning at 5W to strip the residual resist on the film (See Fig. 3 a for detailed parameters)

2.1.4 Lift-off

This is post-etch cleaning step which we call it "lift-off" but in fact is just to strip the post etching resist. The recipe we use for lift-off is soak the sample in **Remover PG for 30mins** and then **sonicate the sample in Acetone for 5mins**. Finally it's transferred to IPA for 2min and blow dry.

2.1.5 Oxidization and Cleaning

To better remove the residuals left on the sample, we first oxidize the sample surface with O2 plasma dose for 1 min (See Fig. 3 d) for detailed parameters) and we use the buffered oxide etcher (BOE) to etch away the formed oxides. The BOE etching consists of 3 steps. First the sample is put in BOE for 10 mins. Then it's transferred to a beaker with DI water for 30s. Finally it's transferred to another beaker with DI water but the sample is kept being rinsed with DI water for 30 seconds.

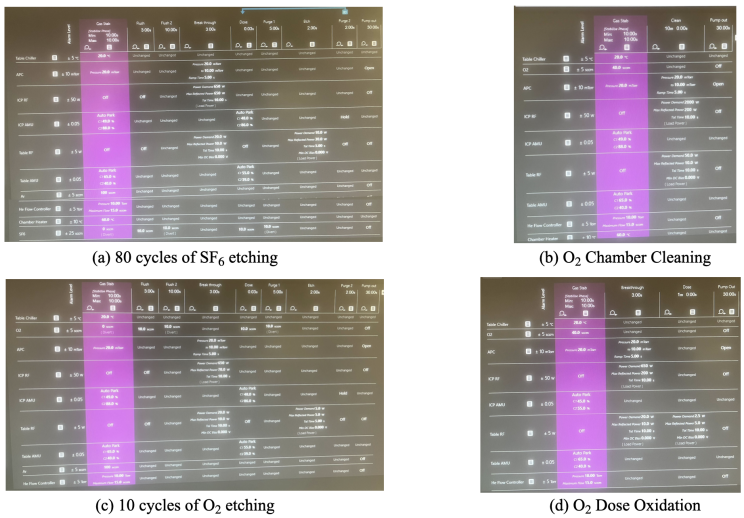

(a) 80 cycles of SF_6 etching

(b) O_2 Chamber Cleaning

(c) 10 cycles of O_2 etching

(d) O_2 Dose Oxidation

Figure 3: Images of the plasma glow during various stages of the Atomic Layer Etching (ALE) process. The panels show: (a) 80 cycles of SF6 plasma for NbN etching, (b) O2 plasma for chamber cleaning, (c) 10 cycles of O2 plasma for resist removal, and (d) an O2 dose for surface oxidation.

2.1.6 Global ALE

In this final step, we did a gentle final etching on the sample surface to get rid of any native oxide formed as they were suggested to be source of decoherence for superconducting devices [1]. We did 5W of O2 etching for 10 cycles and 10W of SF_6 for 8 cycles. Finally we did a O_2 dose for 1min to "seal" the sample with thermal oxides which have less decoherence source than native oxides [1].

2.2 Device Design

For high-kinetic-inductance resonators, there are three key parameters we hope to predict: frequency, impedance and coupling quality factor. We have established analytical and numerical tools for predicting these parameters.

2.2.1 analytical calculations

The kinetic inductance per square of the NbN film can be predicted by its room-temperature resistance per square, given by [5]

$$L_k^{\square} = \frac{\hbar R_N^{\square}}{\pi \Delta_0} \tag{1}$$

where $R_N^{\square}$ is the normal-state sheet resistance, $\hbar$ is the Planck constant divided by 2π, Δ_0 is the superconducting gap energy at zero temperature. For NbN, experimentally it is measured $\Delta_0 \approx 2.08 k_B T_c$ where k_B is the Boltzman constant and T_c is NbN film's critical temperature. For our design, we're interested in designing coplanar waveguide (CPW) resonators as shown in Fig. 4 a. The kinetic inductance per length for a CPW resonator is given by

$$L_k = g \frac{L_k^{\square}}{S} \tag{2}$$

where S is width of the CPW resonator center pin and g is the geometric factor for CPW resonator derived through conformal mappings:

$$g = \frac{\pi}{2}\frac{K(k_0')}{K(k_0)} \tag{3}$$

where $k_0 = \frac{S}{S+2W}$, $k_0' = \sqrt{1-k_0^2}$ and $K(x)$ is the eplliptical integral function. For a CPW resonator, its geometric inductance and capacitance per length is given by

$$C_{geo} = 2\epsilon_0(\epsilon_s - 1)\frac{K(k_1)}{K(k_1')} + 4\epsilon_0\frac{K(k_0)}{K(k_0')} \tag{4}$$

$$L_{geo} = \frac{\mu_0}{4}\frac{K(k_0')}{K(k_0)} \tag{5}$$

where ϵ_0 and μ_0 are vacuum permittivity and permeability, $k_1 = \frac{\sinh(\pi\frac{S}{4h_1})}{\sinh(\pi\frac{S+2W}{4h_1})}$, $k_1' = \sqrt{1-k_1^2}$, h_1 is the substrate height and ϵ_s is the dielectric constant for the substrate ($\epsilon_s = 11.7$ for Si).

Therefore the impedance of the CPW resonator is given by

$$Z = \sqrt{\frac{L_{tot}}{C_{tot}}} = \sqrt{\frac{L_{geo}+L_k}{C_{geo}}} \tag{6}$$

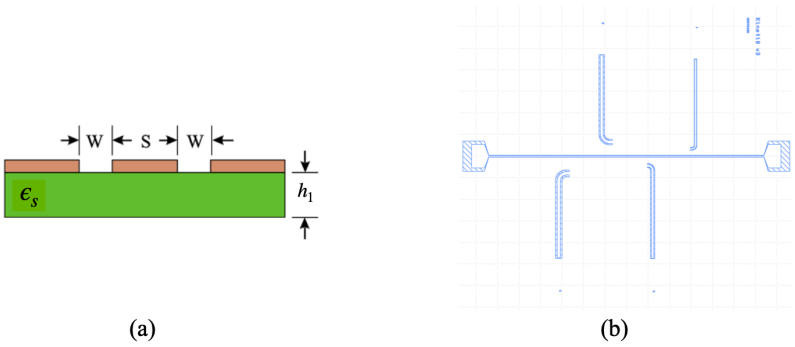

Figure 4: Design schematics for the coplanar waveguide (CPW) resonators. Panel (a) shows a cross-section of the CPW, indicating the center conductor width (S), the gap to the ground planes (W), and the substrate height (h1). Panel (b) displays the layout of a test chip, featuring a central CPW feedline coupled to four individual $\lambda/4$ resonators.

For $\lambda/4$ resonators (voltage node and antinodes on the two termination points), its resonant frequency is given by

$$f_r = \frac{1}{4l\sqrt{(L_{geo}+L_k)C_{geo}}} \tag{7}$$

where l is the length of the $\lambda/4$ resonator. Notice unit of the frequency calcualted from formula above is in Hz not rad $\cdot$ Hz.

2.3 Numerical simulation

Fig. 4 b gives an example of the design of one CPW feedline coupling with 4 CPW resonators. One key parameter is the coupling quality factor between the resonator and feedline, which represents

how much portion of energy will be excited with the resonators during the measurement. The coupling quality factor (Q_c) has to be chosen carefully to match with resonators' internal quality factor (Q_i) to extract Q_i with best accuracy. Q_c geometrically is decided by two parameters as shown in Fig. 5 b: the coupling arm legnth and coupling gap length. Intuitively, the longer the coupling arm or the shorter the coupling gap, the stronger the coupling (the lower the Q_c). Analytical derivations have been performed to derive Q_c for CPW resonators coupled with CPW feedlines [2] but in our case, with kinetic inductance present, the analytical solution becomes too complicated. Instead, we use Sonnet, a commercial microwave simulation software with the capability of simulating 2D planar circuits with customized sheet inductance layer defined. By simulating the S12 parameter in the design, we could extract resonator's coupling quality factor. Below are the procedures for the Sonnet simulation

- **Import the design**: we use python CAD desgin packages such as shapely and gdspy to generate the mask design and we use pysonnet, a python interface package for automating the design import process [11].
- **Simulation setting**: Fig. 5 c shows the critical settings for running the sonnet simulation. The inductance per square should be altered accordingly based on the predicted kinetic inductance of the film.
- **Adaptive Sweep around estimated frequency**: Because high Q_c causes a narrow resonance and is computationally costly to simulate. Our strategy is to start with small Q_c, i.e. increase the coupling arm length or reduce the coupling gap width and first run the Adaptive Sweep (ABS) mode of simulation in Sonnet to pin down the frequency first. The Sonnet ABS doesn't do a good job for band greater than 1GHz so we typically analytically estimate the frequency and run a 1GHz band ABS simulation around that frequency.
- **Zoom-in with Linear Sweep**: After we pin down the frequency, we can increase the coupling gap width and decrease coupling arm length and use linear sweep mode across a smaller frequency band. Usually linear sweep is much slower than ABS so we only use linear until ABS cannot find the mode anymore.
- **Fit the Real-Imaginary part of S12 to extract** Q_c: Finally, we extract the Q_c by fitting the simulated real and imaginary part of the S12 data. Fig. 5 d shows the result of the simulation

3 Results and Discussion

3.1 Etch Rate Characterization

To do an etching rate characterization, we first pattern 3 rows of squares on our NbN film. Then we do lithography to mask off all but one row and etch these rows for varying numbers of cycles. Then we evaluate these chips under AFM to measure film thickness, we then fit this data to compute our Etch Rate. The raw numbers are shown in Figure 6.

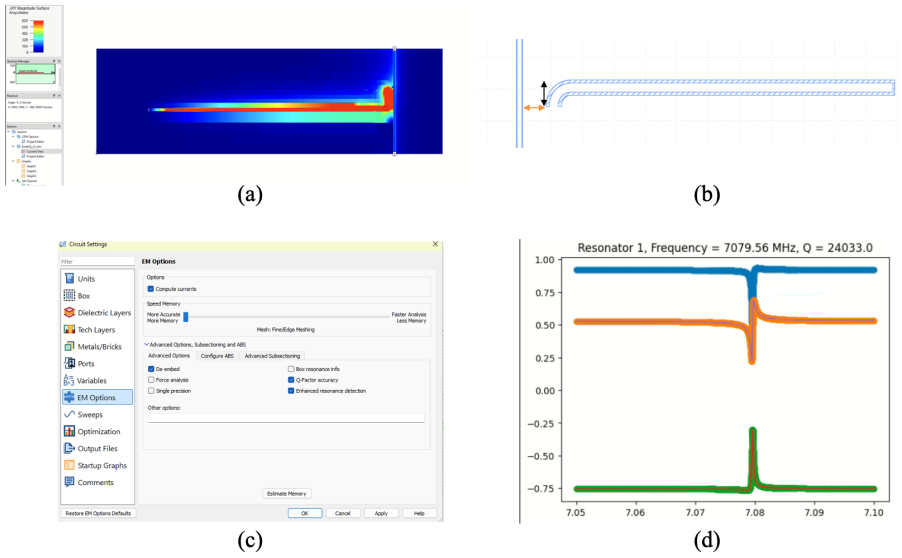

Figure 5: Numerical simulation process and results using Sonnet software. Panel (a) shows the simulated current distribution. Panel (b) indicates the key geometric features that determine the coupling strength: the coupling arm length (black arraow) and gap length (orange arrow). Panel (c) is a screenshot of the critical simulation settings. Panel (d) presents the simulated S12 response of a resonator, with a fit used to extract a coupling quality factor (Qc) and resonant frequency.

3.2 Surface Morphology

3.2.1 Surface Roughness Study

We use AFM to study the surface roughness and mainly to compare before and after etching and before and after cleaning step. As Fig. 7 a shows, before the process, the raw NbN film has surface roughness less than 1nm across 1μm $\times$ 1μm area and there are larger scale film thickness variation on the order of 5-10nm over area of 20μm $\times$ 20μm area. This smoothness over small area is probably due to the ALD growth technique and the long scale variation could be caused by the lattice mismatch between Si and NbN (we later found this variation is less pronounced on the NbN grown on sapphire wafer). After etching, and without oxidation and BOE cleaning, we can see there are many 20nm tall and a few hundred nm wide spikes occurred on the NbN surface as shown in Fig. 7 b. We suspect these spikes could be cause by residual resist left on the film. Similar spikes also show up on the Si surface after etching as shown in Fig. 8 a. In Fig. 7 c, after the oxidation and BOE cleaning step, we can see that the density of the spikes on NbN has decreased significantly and the microscopic roughness has maintained about the same as before etching. Fig. 8 b shows less spikes after cleaning on Si too though the surface show smaller but denser spikes afterwards.

3.2.2 Overetching

As we previously characterized, since the etch rate of Si is much faster than NbN, the overetch into the Si is unavoidable. To characterize the overetching depth into the Si, we performed the AFM at the trench region of the Si resonator to measure the depth of the trench. Fig. 9 shows the result that the total measured depth are 45nm and 25nm for two resonators of different gap widths (20

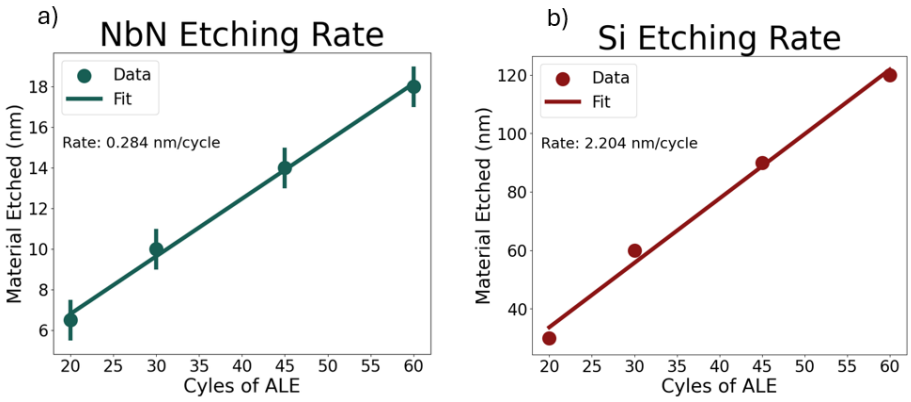

Figure 6: The Etching Rate of NbN and Si as calibrated with our AFM data.

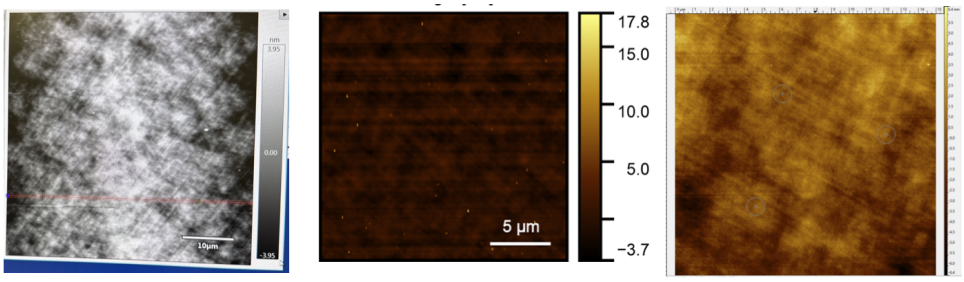

Figure 7: Atomic Force Microscopy (AFM) images comparing the surface morphology of the Niobium Nitride (NbN) film at different fabrication stages. (a) The smooth surface of the as-deposited NbN film. (b) The surface after etching, showing numerous tall spikes attributed to residual resist. (c) The surface after an oxidation and BOE cleaning step, which significantly reduced the density of spikes while maintaining low microscopic roughness.

and 40μm) after 80 cycles of etching on the same chip. Later through microwave measurement and kinetic inductance calculation, we find the NbN film thickness is about 15nm so the Si overetching is 30 and 10nm for te two resonator design and suggests the overetching rate depends on the gap size

3.3 Cryogenic Microwave Measurement results

The samples that we designed were measured in a dilution refrigerator, which is capable of reaching a base temperature of 7 mK. During the first phase of the cooldown, we performed a 4-point measurement of the Hall bar to determine the resistance of the film and its critical temperature (the temperature at which the material returns to its normal state).

This allows us to use the Mattis-Bardeen relation given in Equation 1, to estimate the kinetic inductance per square that we expect. From the data shown in Figure 10 we see that

1. $T_C = 10.9K$
2. $R_N = 300\ \Omega/\square$

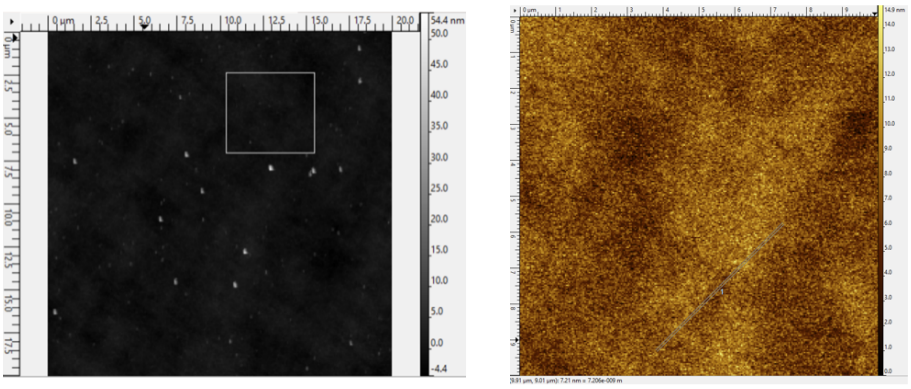

(a) (b)

Figure 8: Atomic Force Microscopy (AFM) images of the silicon (Si) surface adjacent to the resonator. (a) The Si surface after the etching process, revealing the presence of spikes. (b) The Si surface after cleaning, showing a changed morphology with smaller but more densely packed spikes.

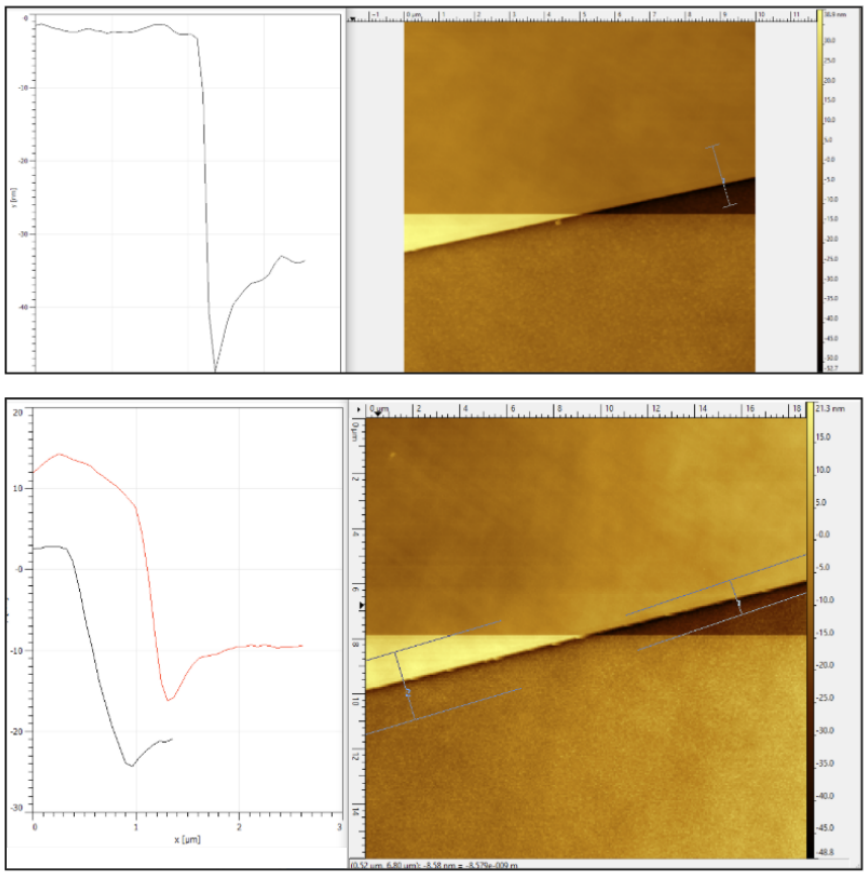

Figure 9: Atomic Force Microscopy (AFM) measurements characterizing the over-etching into the silicon substrate. The line profiles and corresponding 3D images show the trench depths for two different resonator gap widths after 80 cycles of the etching process.

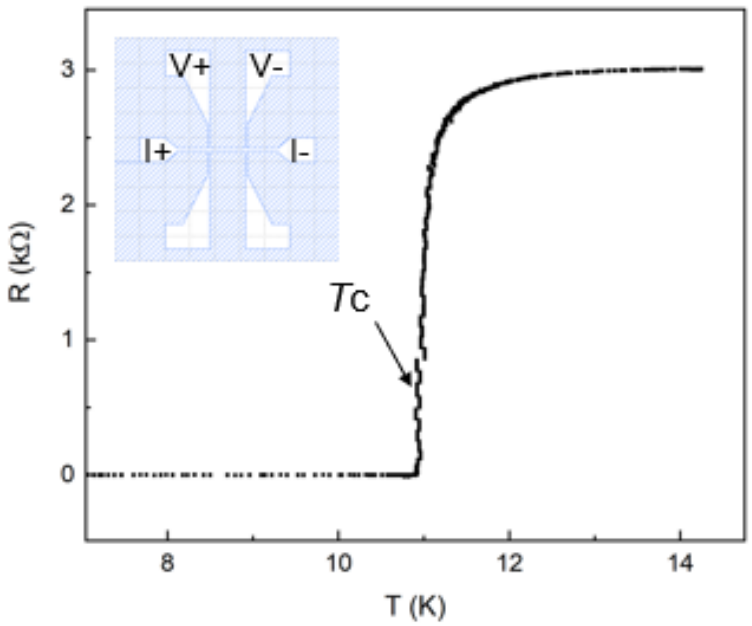

Figure 10: Here we show the resistance of our Hall Bar (inset in top left) as a function of temperature. The temperature at which the resistance drops to 0 is the critical temperature T_C. The resistance value of the film right before this transition is known as R_N or the normal state resistance.

Number	Frequency (GHz)	Coupling Q	Internal Q
1	3.576 GHz	7.2×10^3	1.2×10^6
2	3.877 GHz	2.7×10^3	6.9×10^4
3	4.153 GHz	2.2×10^3	3.5×10^4
4	4.409 GHz	1.9×10^3	3.4×10^4

Table 1: Measured Frequencies and Quality Factors for our resonators.

3. $L_K = 36\ pH/\square$

To do these measurements, we had to operate our dilution refrigerator in the 8 K- 15 K regime. However, due to the abundance of thermal quasiparticles, this will degrade the quality factor. Next, we cooled our dilution refrigerator to its base temperature of 7 mK and began measuring our resonators. We found the frequencies of the four resonators on our sample which are shown in Table 1 along with the fits for the external and coupling quality factors the raw data and fitting errors are shown for all of the resoantors in Figure11. The fitting was done using the standard algorithm of circle fitting described in [7].

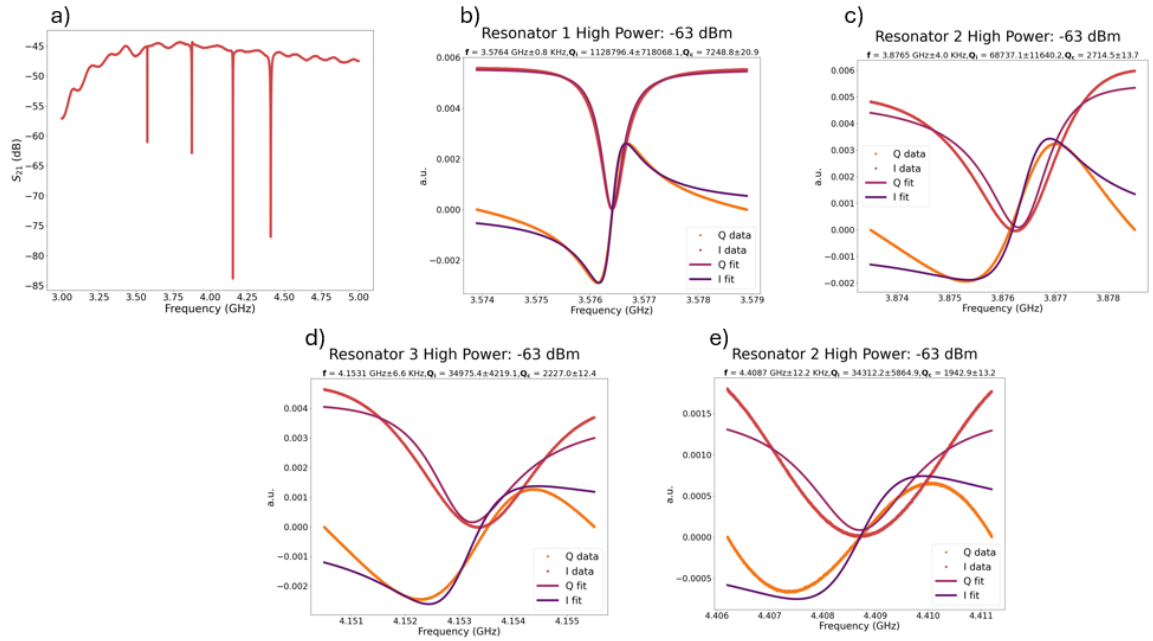

Figure 11: Panel a) shows a broad sweep in frequency, which allows us to see all four modes. Panels b)-e) show the measured in-phase (I/Re) and out-of-phase (Q/Im) response of the resonators in a 1 MHz span around their resonance.

3.3.1 Quality Factor

To unpack the measurement a little further, we can briefly discuss the meaning behind the quality factor. When we have a resonant circuit the Quality Factor is defined as:

$$Q = \omega_0 \frac{\text{Average Energy Stored}}{\text{Average Energy Lost}} \tag{8}$$

and can roughly be thought of as a proxy for how long energy can be stored in the resonator. For quantum information applications, the quality factor is of utmost importance since it determines how long energy can be stored in a system.[1] Now, if we have a resonant circuit, we have to couple it to another object (in our case, a transmission line) to measure it. Therefore, we can define:

$$Q_c = \frac{\omega_0}{\kappa_c} \tag{9}$$

where κ_c is the rate at which energy/information leaks out of our resonator. This parameter is known as our coupling Q. Another fact about quality factors is that they add like resistors in parallel:

$$\frac{1}{Q_T} = \sum_i \frac{1}{Q_i} \tag{10}$$

this can be rigorously shown using a circuit model as done in Pozar[6]. One lesson we can take away from Equation 10 is that the total Q factor of your resonator will always be limited by the

[1]Recall that the major premise of quantum mechanics is that energy is quantized, thus if we want to study the behavior of single quanta of energy they must be present for a while.

most lossy element of your system. Another lesson in a similar vein is that if your resonator is very strongly coupled to the outside work (i.e, your feedline) then it will inherit a lot of loss from the environment. This is one of the reasons why we suspect the internal quality factors of our resonators were so low. Finally, we ideally would like our resonators to have the same internal and coupling quality factors. The reasoning for this is that as stated before, overcoupled resonators (ones where the coupling quality factor is much smaller than the internal one) are susceptible to being perturbed by the environment. However, undercoupled resonators leak out their radiation too slowly making it very difficult to resolve their presence.

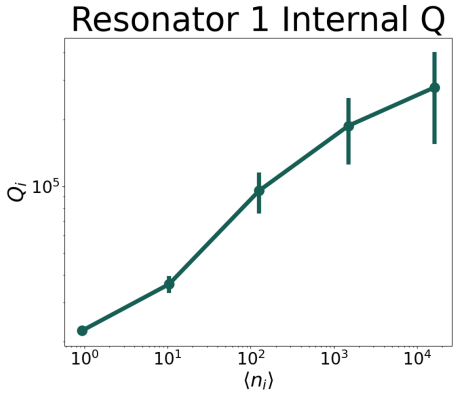

Figure 12: The internal Quality factor for one of the resonators as a function of power. The quality factor increases as a function of power, indicating strong coupling to environmental TLS. The error bars also increase as a function of power since the resonator is very overcoupled.

3.3.2 Power Dependence

One way in which the quality factor of resonators can be reduced is by using two-level systems (TLS). These are fluctuators that couple to the electromagnetic mode and can cause loss. As you increase the power, eventually these two-level systems stop dissipating power since they have all been saturated into their excited state. As such, measuring the Q of superconducting resonators as a function of power allows one to determine how strongly the resonator is coupled to these TLS. Since our resonators were very overcoupled, we expected them to be strongly coupled to many TLS. Therefore, we only did the power sweep for one of the resonators, the one with the lowest coupling Q. The results are shown in Figure 12.

4 Conclusion and Future Outlook

We have demonstrated a reproducible, CMOS-compatible workflow that produces ultra-smooth, high-Q niobium-nitride resonators by combining calibrated SF/O atomic-layer etching with a post-etch oxidation and BOE cleaning sequence. This approach offers angstrom-scale thickness control and preserves pristine sidewalls, allowing room-temperature sheet resistance to serve as a reliable predictor of kinetic inductance. When linked to Sonnet electromagnetic simulations, this predictive framework enables accurate targeting of resonance frequencies, impedances, and external coupling strengths. Devices fabricated with 20 nm NbN on silicon achieved high-power internal quality factors of approximately one million at millikelvin temperatures, confirming that the low-loss potential of ultrathin NbN can be retained in practical microwave circuits.

Looking ahead, migrating the process to low-loss substrates such as sapphire or high-resistivity silicon should further suppress dielectric participation and push quality factors toward one million at single photon power. Blanket atomic-layer "thinning" offers a post-growth knob for setting kinetic inductance with sub-picohenry-per-square precision, facilitating impedance-matched resonator networks and superinductors. Finally, eliminating residual resist contamination, refining oxygen dosing, and incorporating surface encapsulation method will help quench two-level-system loss and reduce power dependence.

References

[1] Mustafa Bal et al. "Systematic improvements in transmon qubit coherence enabled by niobium surface encapsulation". In: *npj Quantum Information* 10.1 (Apr. 2024), p. 43. ISSN: 2056-6387. DOI: 10.1038/s41534-024-00840-x. URL: https://doi.org/10.1038/s41534-024-00840-x.

[2] Ilya Besedin and Alexey P. Menushenkov. "Quality factor of a transmission line coupled coplanar waveguide resonator". In: *EPJ Quantum Technology* 5 (Jan. 2018). ISSN: 2196-0763. DOI: 10.1140/epjqt/s40507-018-0066-3. URL: https://epjquantumtechnology.springeropen.com/articles/10.1140/epjqt/s40507-018-0066-3.

[3] S. P. Harvey et al. "Coupling two spin qubits with a high-impedance resonator". en. In: *Physical Review B* 97.23 (June 2018), p. 235409. ISSN: 2469-9950, 2469-9969. DOI: 10.1103/PhysRevB.97.235409. URL: https://link.aps.org/doi/10.1103/PhysRevB.97.235409.

[4] Han-Byul Jang, Ji Soo Lim, and Chan-Ho Yang. "Film-thickness-driven superconductor to insulator transition in cuprate superconductors". en. In: *Scientific Reports* 10.1 (Feb. 2020), p. 3236. ISSN: 2045-2322. DOI: 10.1038/s41598-020-60037-y. URL: https://www.nature.com/articles/s41598-020-60037-y.

[5] David Niepce, Jonathan Burnett, and Jonas Bylander. "High Kinetic Inductance NbN Nanowire Superinductors". In: *Phys. Rev. Appl.* 11 (4 Apr. 2019), p. 044014. DOI: 10.1103/PhysRevApplied.11.044014. URL: https://link.aps.org/doi/10.1103/PhysRevApplied.11.044014.

[6] David M. Pozar. *Microwave engineering*. 4th ed. Hoboken, NJ: Wiley, 2012. ISBN: 9780470631553.

[7] S. Probst et al. "Efficient and robust analysis of complex scattering data under noise in microwave resonators". In: *Review of Scientific Instruments* arXiv:1410.3365 (Oct. 2014). arXiv:1410.3365. DOI: 10.48550/arXiv.1410.3365. URL: http://arxiv.org/abs/1410.3365.

[8] Emma L. Rosenfeld et al. "High-Fidelity Two-Qubit Gates between Fluxonium Qubits with a Resonator Coupler". en. In: *PRX Quantum* 5.4 (Nov. 2024), p. 040317. ISSN: 2691-3399. DOI: 10.1103/PRXQuantum.5.040317. URL: https://link.aps.org/doi/10.1103/PRXQuantum.5.040317.

[9] Calder Sheagren et al. "Atomic Layer Deposition Niobium Nitride Films for High-Q Resonators". In: arXiv:1908.07146 (Dec. 2019). arXiv:1908.07146. DOI: 10.48550/arXiv.1908.07146. URL: http://arxiv.org/abs/1908.07146.

[10] Mingrui Xu et al. "Magnetic Field-Resilient Quantum-Limited Parametric Amplifier". en. In: *PRX Quantum* 4.1 (Feb. 2023), p. 010322. ISSN: 2691-3399. DOI: 10.1103/PRXQuantum.4.010322. URL: https://link.aps.org/doi/10.1103/PRXQuantum.4.010322.

[11] Nicholas Zobrist. *pysonnet: Python tools for working with Sonnet E&M data*. Version 0.0.4. MIT License; accessed 2025-06-12. 2023. URL: https://github.com/zobristnicholas/pysonnet.